



## Original article

Discovery of the first inhibitors of bacterial enzyme D-aspartate ligase from *Enterococcus faecium* (Asl<sub>fm</sub>)

Veronika Škedelj<sup>a</sup>, Andrej Perdih<sup>b,\*\*</sup>, Matjaž Brvar<sup>b</sup>, Ana Kroflič<sup>c</sup>, Vincent Dubbée<sup>d,e,f,g,h,i,j</sup>, Victoria Savage<sup>m</sup>, Alex J. O'Neill<sup>m</sup>, Tom Solmajer<sup>b</sup>, Marija Bešter-Rogač<sup>c</sup>, Didier Blanot<sup>k,l</sup>, Jean-Emmanuel Hugonnet<sup>d,e,f,g,h,i,j</sup>, Sophie Magnet<sup>d,e,f,g,h,i,j,1</sup>, Michel Arthur<sup>d,e,f,g,h,i,j</sup>, Jean-Luc Mainardi<sup>d,e,f,g,h,i,j</sup>, Jure Stojan<sup>n</sup>, Anamarija Zega<sup>a,\*</sup>

<sup>a</sup> Faculty of Pharmacy, University of Ljubljana, Aškerčeva 7, 1000 Ljubljana, Slovenia

<sup>b</sup> National Institute of Chemistry, Hajdrihova 19, 1000 Ljubljana, Slovenia

<sup>c</sup> Faculty of Chemistry and Chemical Technology, University of Ljubljana, Aškerčeva 5, 1000 Ljubljana, Slovenia

<sup>d</sup> Centre de Recherche des Cordeliers, LRMA, Equipe 12, Université Pierre et Marie Curie, Paris 6, UMR S 872, Paris F-75006 France

<sup>e</sup> INSERM, U872, Paris F-75006 France

<sup>f</sup> Université Paris Descartes, Sorbonne Paris Cité, UMR S 872, Paris F-75006 France

<sup>g</sup> Institut Parisien de Chimie Moléculaire, équipe GOBS, Université Pierre et Marie Curie, Paris 6, France

<sup>h</sup> Centre National de la Recherche Scientifique, UMR 7201, Paris F-75006 France

<sup>i</sup> AP-HP, Hôpital Européen Georges Pompidou, Paris F-75015 France

<sup>j</sup> Rhode Island Hospital, Brown University, Providence, RI 02903–4923, USA

<sup>k</sup> Laboratoire des Enveloppes Bactériennes et Antibiotiques, University Paris-Sud, IBBMC, UMR 8619, 91405 Orsay, France

<sup>l</sup> CNRS, 91405 Orsay, France

<sup>m</sup> Antimicrobial Research Centre and School of Molecular & Cellular Biology, University of Leeds, Leeds LS2 9JT, UK

<sup>n</sup> Institute of Biochemistry, Medical Faculty, University of Ljubljana, Vrazov trg 2, 1000 Ljubljana, Slovenia

## ARTICLE INFO

## Article history:

Received 28 February 2013

Received in revised form

1 June 2013

Accepted 2 June 2013

Available online 28 June 2013

## Keywords:

D-Aspartate ligase

*Enterococcus faecium*

ATP binding site

Pharmacophore modeling

Kinetic measurements

Isothermal titration calorimetry

Antibacterial agents

Drug design

## ABSTRACT

The D-aspartate ligase of *Enterococcus faecium* (Asl<sub>fm</sub>) is an attractive target for the development of narrow-spectrum antibacterial agents that are active against multidrug-resistant *E. faecium*. Although there is currently little available information regarding the structural characteristics of Asl<sub>fm</sub>, we exploited the knowledge that this enzyme belongs to the ATP-grasp superfamily to target its ATP binding site. In the first design stage, we synthesized and screened a small library of known ATP-competitive inhibitors of ATP-grasp enzymes. A series of amino-oxazoles derived from bacterial biotin carboxylase inhibitors showed low micromolar activity. The most potent inhibitor compound **12**, inhibits Asl<sub>fm</sub> with a  $K_i$  value of 2.9  $\mu$ M. In the second design stage, a validated ligand-based pharmacophore modeling approach was used, taking the newly available inhibition data of an initial series of compounds into account. Experimental evaluation of the virtual screening hits identified two novel structural types of Asl<sub>fm</sub> inhibitors with 7-amino-9H-purine (**18**) and 7-amino-1H-pyrazolo[3,4-d]pyrimidine (**30** and **34**) scaffolds, and also with  $K_i$  values in the low micromolar range. Investigation the inhibitors modes of action confirmed that these compounds are competitive with respect to the ATP molecule. The binding of inhibitors to the target enzyme was also studied using isothermal titration calorimetry (ITC). Compounds **6**, **12**, **18**, **30** and **34** represent the first inhibitors of Asl<sub>fm</sub> reported to date, and are an important step forward in combating infections due to *E. faecium*.

© 2013 Elsevier Masson SAS. All rights reserved.

**Abbreviations:** ATP, adenosine-5'-triphosphate; ITC, isothermal titration calorimetry; MIC, minimal inhibitory concentration; RA, residual activity; PDB, Protein databank; SARs, structure–activity relationships.

\* Corresponding author. Tel.: +386 1 4769 673; fax: +386 1 4258031.

\*\* Corresponding author. Tel.: +386 1 4760 376; fax: +386 1 4760300.

E-mail addresses: [andrej.perdih@ki.si](mailto:andrej.perdih@ki.si) (A. Perdih), [anamarija.zega@ffa.uni-lj.si](mailto:anamarija.zega@ffa.uni-lj.si) (A. Zega).

<sup>1</sup> Present address: INSERM U1070, Laboratoire de Pharmacologie des Anti-infectieux, Université de Poitiers, Pôle Biologie Santé, 1 rue Georges Bonnet, 86022 Poitiers, BP633, France.

## 1. Introduction

Despite the relentless increase in resistance to antimicrobial agents of the most important pathogens, the number of new antibiotics approved for clinical use has shown a remarkable decline over the past two decades. Enterococci are one of the most important pathogens for problems of resistance, and particularly *Enterococcus faecium*, which belongs to the group of 'ESKAPE' pathogens that currently cause the majority of nosocomial infections [1,2].

Enterococci are among the most prevalent pathogens that have developed resistance to vancomycin, the so-called antibiotic of last resort. Vancomycin targets the bacterial cell wall by forming complexes with peptidoglycan precursors, thereby inhibiting peptidoglycan biosynthesis [3]. Since the first reported cases of vancomycin-resistant *E. faecium* in 1988, enterococcal resistance to vancomycin has dramatically increased [4].

Bacterial peptidoglycan is an attractive drug target, as it completely surrounds the bacterial cytoplasmic membrane and thus provides mechanical protection against the turgor pressure of the cytoplasm. It also serves as an attachment site for various surface polymers that interact with host cells and the immune system, and it is involved in cell division [5,6]. Peptidoglycan is a polymeric structure that is composed of  $\beta$ -linked *N*-acetylglucosamine (GlcNAc) and *N*-acetylmuramic acid (MurNAc) polysaccharide chains, which are cross-linked through variable peptide stems. The polymerization process is performed by glycosyltransferases that catalyze the formation of  $\beta$ -1,4 bonds, and  $D,D$ -transpeptidases that cross-link the glycan strands [7]. The peptidoglycan assembly pathway involves a wide range of other bacterial enzymes that act at three distinct sites in the bacterial cell: the cytoplasm, and the inner and outer sides of the cytoplasmic membrane.

The synthesis of the UDP-MurNAc-pentapeptide precursor of peptidoglycan begins in the cytoplasm and involves six Mur enzymes (MurA to MurF). The first two of these (MurA and MurB) catalyze the formation of UDP-MurNAc, onto which the following four enzymes (MurC to MurF) subsequently add five amino acids, with alternating *L*- and *D*-configurations except for terminal *D*-Ala-*D*-Ala [8]. The pathogenic Gram-positive bacteria of the genera *Staphylococcus*, *Streptococcus* and *Enterococcus* have a conserved *L*-alanyl- $\gamma$ -*D*-glutamyl-*L*-lysyl-*D*-alanyl-*D*-alanine peptide stem onto which a variable side chain is linked to the  $\epsilon$ -amino group of *L*-Lys [3,5,9]. The side chain consists of one to seven amino acids from both the *L*- and *D*-series. The activation of *L*-amino acids and glycine for incorporation into the peptide side-chain is performed by aminoacyl-tRNA synthetases, which form aminoacyl-tRNAs that are then transferred to the precursors by the enzymes of the Fem transferase family [10,11].

While members of the Fem family have been extensively studied and characterized, the incorporation of *D*-amino acids into peptidoglycan precursors has not been well explored. The *E. faecium* *D*-aspartate ligase, Asl<sub>fm</sub>, which was partially purified in

1972 (Fig. 1), activates *D*-aspartic acid as  $\beta$ -aspartyl-phosphate in an ATP-dependent reaction, and links the activated amino acid to the  $\epsilon$ -amino group of *L*-Lys in the cytoplasmic precursor UDP-MurNAc-pentapeptide (Fig. 2) [12,13]. Structural studies have also indicated that in the mature peptidoglycan of *E. faecium*, the  $\alpha$ -carboxyl group of the *D*-aspartic acid is partly amidated (*D*-iso-asparagine) [5,9].

The gene encoding the *D*-aspartate ligase in *E. faecium* (Asl<sub>fm</sub>) has been identified and enzyme activity was assessed following purification of the protein overexpressed in *Escherichia coli*. The structure of hexapeptide product of Asl<sub>fm</sub> was determined by tandem mass spectroscopy [14]. The *asl*<sub>fm</sub> gene was also expressed in *Enterococcus faecalis* to demonstrate the catalytic activity of Asl<sub>fm</sub> *in vivo*. Analysis of the specificity of Asl<sub>fm</sub> for its amino acid substrate shows that the enzyme is highly specific for *D*-Asp since increase in the length of the side chain or substitution of the  $\alpha$ -amino group by a hydroxyl group were not tolerated by the enzyme. *D*-iso-asparagine did not serve as a substrate for the enzyme, which indicates that its presence in the cross-linking of *E. faecium* originates from amidation of the  $\alpha$ -carboxyl group after incorporation into precursors by Asl<sub>fm</sub> [14].

Close homologs of Asl<sub>fm</sub> can be found in the genomes of 10 bacterial species that can produce precursors substituted by *D*-Asp, but there are none in bacteria that contain directly cross-linked peptidoglycan or side-chains containing *L*-amino acids and glycine. Low-level sequence similarity has indicated that Asl<sub>fm</sub> is a member of the ATP-grasp superfamily [14], which is characterized by an unusual nucleotide-binding fold: the ATP-grasp fold. Enzymes of this family catalyze the formation of a carbon–nitrogen bond by a common reaction mechanism, which requires Mg<sup>2+</sup> and ATP for the formation of an acylphosphate intermediate. The protein superfamily includes biotin carboxylase, glutathione synthetase, carbamoyl phosphate synthetase, ribosomal protein S6 modification enzyme (RimK), urea amidolyase, tubulin-tyrosine ligase, and three enzymes of purine biosynthesis [15]. Additional members include *D*-alanine:*D*-alanine ligase and the closely-related *D*-Ala-*D*-lactate-forming and *D*-Ala-*D*-Ser-forming enzymes found in glycopeptide-resistant Gram-positive bacteria. Aside from Asl<sub>fm</sub>, these are the only known members of the family that are involved in peptidoglycan synthesis [16].

As Asl<sub>fm</sub> belongs to the ATP-grasp superfamily, this aided our efforts in the development of what are, to the best of our knowledge, the first inhibitors of this target. Our two-stage drug design process and the biochemical and biophysical characterization are depicted in Scheme 1. In the first stage, we designed and screened a small library of known ATP-competitive inhibitors of bacterial members of the ATP-grasp superfamily. Among these, there were amino-oxazoles that inhibited the target enzyme Asl<sub>fm</sub> with *K*<sub>i</sub> values in the low micromolar range. In the next design phase of our investigation, a ligand-based pharmacophore model was built using the available data that relate to the inhibitory action of the initial series, in order to identify novel inhibitors of the target enzyme that have different scaffolds. This approach enabled us to

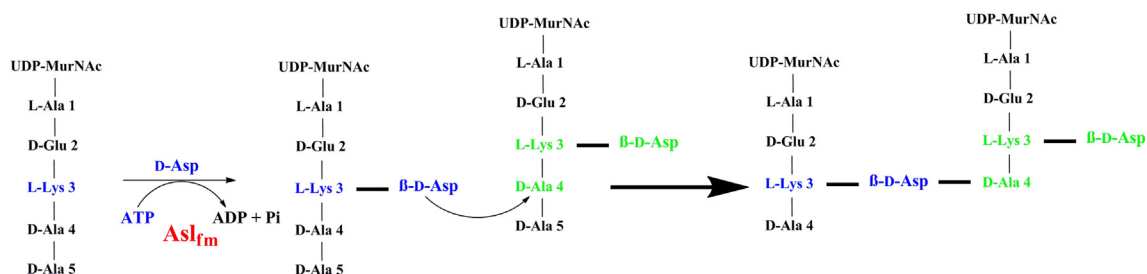


Fig. 1. Function of Asl<sub>fm</sub> in peptidoglycan cross-bridge formation in *E. faecium*.

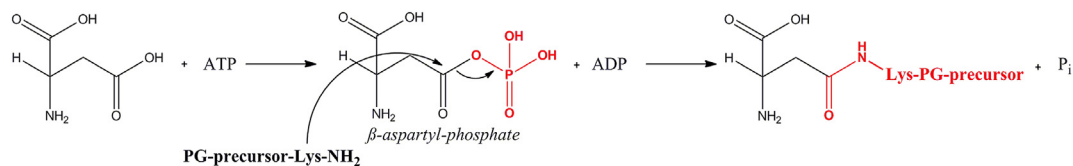


Fig. 2. Reaction catalyzed by AsI<sub>fm</sub>.

discover novel classes of AsI<sub>fm</sub> inhibitors that were further studied and characterized by isothermal titration calorimetry. For selected compounds, we also evaluated the antimicrobial activity.

## 2. Results and discussion

### 2.1. Design stage 1: design and synthesis of amino-oxazoles and amino-thiazoles, starting from inhibitors of members of the ATP-grasp enzyme superfamily

Due to the currently limited knowledge relating to the structural characteristics of our target enzyme, we took advantage of the only known specific of the 3D structure of AsI<sub>fm</sub>: its affiliation to the ATP-grasp superfamily of enzymes [14]. In many cases, although there is no significant primary sequence homology between the enzymes, the structures of their ATP-binding domains are largely superimposable [17].

Based on this information, we first, synthesized and screened a small library of known ATP-competitive inhibitors **5–7** of the bacterial biotin carboxylase which is also a member of the same ATP-grasp superfamily of enzymes (Table 1) [18]. Evaluation of their biological activities against purified AsI<sub>fm</sub> using a pyruvate kinase–lactate dehydrogenase detection system revealed a promising inhibitor of the target enzyme (compound **6**, Fig. 3A, Table 1). As the aromatic moiety turned out to be important for the inhibitory activity, our next objective was the incorporation of more electron-rich amines, to enable additional potential interactions with the AsI<sub>fm</sub> active site. Thus, we synthesized seven target compounds **8–12** (Table 1), with these characteristics. Finally, the amino-oxazole moiety was replaced by two amino-thiazoles, as these were commercially available (compounds **13** and **14**, Table 1).

The synthesis of the compounds reported in the present study is outlined in Scheme 2. In the first step, hydrolysis of ethyl esters with 2–5.2 equivalents of sodium hydroxide provided oxazole (**1**) and thiazole (**2** and **3**) acids. These were subsequently converted to target compounds **5–14** using TBTU-promoted coupling with commercially available primary or secondary amines. For compound **12**, the appropriate secondary amine **4** was obtained prior to the coupling reaction, by sodium cyanoborohydride-effected

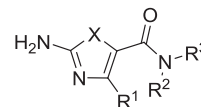
reductive amination of (1*H*-indol-5-yl)methanamine with 3,5-dibromobenzaldehyde (Scheme 2).

All of these synthesized compounds (Table 1) were assayed for *in-vitro* inhibitory activity toward recombinant AsI<sub>fm</sub> using a pyruvate kinase–lactate dehydrogenase enzymatic assay [19–21]. The results for the whole series are presented as residual activities (RAs) of the enzyme in the presence of 50 or 100 μM of the target compounds, and as *K<sub>i</sub>* values with respect to ATP for the most active compounds (Table 1).

With a *K<sub>i</sub>* of 44 μM, compound **6** represents the first known inhibitor of our target enzyme AsI<sub>fm</sub> (Table 1), and it was therefore

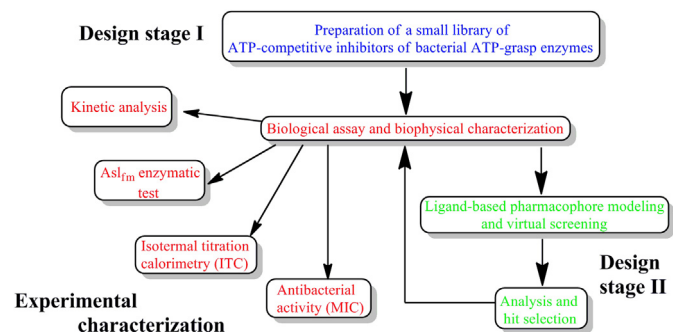
Table 1

Inhibitory activities of amino-oxazoles (**5–12**) and amino-thiazoles (**13–14**) against AsI<sub>fm</sub>.



Cmpd	X	R <sup>1</sup>	R <sup>2</sup>	R <sup>3</sup>	RA [%] <sup>a</sup>
<b>5</b>	O	H			75
<b>6</b>	O	H			43 <i>K<sub>i</sub></i> = 44 μM
<b>7</b>	O	H			94
<b>8</b>	O	H			74
<b>9</b>	O	H			98
<b>10</b>	O	H		H	90
<b>11</b>	O	H		H	79
<b>12</b>	O	H			44* <i>K<sub>i</sub></i> = 2.9 μM
<b>13</b>	S	H			80
<b>14</b>	S	CH <sub>3</sub>			82

<sup>a</sup> Residual activity (RA, %) of the enzyme at 250 μM of the tested compounds, except for compound **12** marked with \*, which was tested at 100 μM due to limited solubility. Data are means of two independent experiments. Standard deviations were within ±10% of the mean.



Scheme 1. Outline of the design steps and subsequent biochemical and biophysical characterization of the hit compounds used in this study.

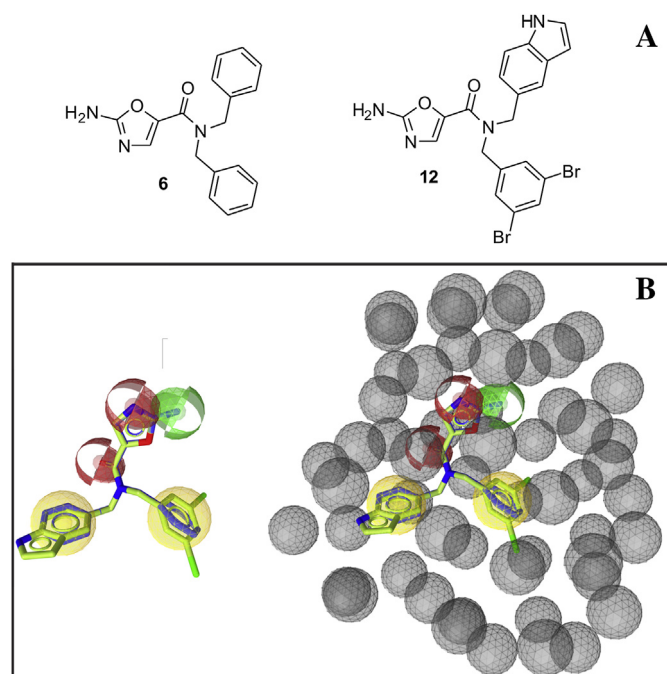


**Fig. 3.** (A) Chemical structures of the amino-oxazole compounds **6** and **12** used for the construction of the ligand-based pharmacophore model. (B) Active compounds **6** and **12** aligned with the derived ligand-based pharmacophore model. The green sphere represents the hydrogen bond donor, the two red spheres the hydrogen bond acceptors. The two yellow spheres denote hydrophobic pharmacophoric features (left), and the derived pharmacophore model with exclusion volumes is depicted as gray spheres (right). (For interpretation of the references to color in this figure legend, the reader is referred to the web version of this article.)

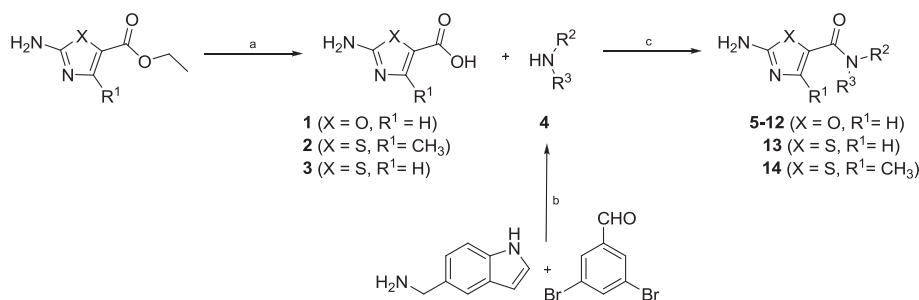
an important starting point for the further design and optimization of these  $AsI_{fm}$  inhibitors. Based on compounds **5–7** [18], and promising initial inhibition data, we developed and synthesized a focused library of additional seven target compounds (compounds **8–14**; Table 1), to establish further structure–activity relationships (SARs). The data from the enzymatic inhibition assay clearly showed that for retention of inhibitory activity toward the target enzyme, secondary amines with aromatic substituents must be coupled to 2-amino-1,3-oxazole-5-carboxylic acid. If primary heterocyclic amines were coupled instead, the enzymatic inhibitory activity significantly decreased (compound **11**) or was even lost (compound **10**). Replacing one phenyl ring with the aliphatic butyl group (compound **5**) resulted in very modest inhibition of  $AsI_{fm}$ , whereas dibutylamine derivative **7** was devoid of  $AsI_{fm}$  inhibitory activity. To retain aromatic substituents and possibly obtain an additional hydrogen bond between the compound and target

enzyme, we replaced both phenyl rings by the pyridine moiety (compound **8**). However, the enzymatic inhibitory activity was significantly decreased or was lost. This was the case for *N*-(pyridin-4-ylmethyl)ethanamine derivative **9**, where only one pyridine ring was introduced into the molecule. The introduction of two bromine atoms on one phenyl ring and the replacement of another phenyl moiety with indole led to the most potent inhibitor of  $AsI_{fm}$  of this series: compound **12**, with a  $K_i$  of 2.9  $\mu$ M. Finally, compounds containing a thiazole ring (**13** and **14**) did not show any significant inhibition of the target enzyme.

## 2.2. Design stage 2: ligand-based pharmacophore modeling approach and virtual screening directed toward novel chemical classes of $AsI_{fm}$ inhibitors

Pharmacophore modeling is a widely used method in modern drug discovery [22,23], and it is particularly useful when the three-dimensional (3D) structure of the target has not been described. Several software tools are available to derive 3D pharmacophore models in an automated fashion. LigandScout is an established structure-based or ligand-based pharmacophore generator, and it was used for the pharmacophore modeling part of the present study [24].

To begin with, two active compounds, **6** and **12** (Fig. 3A), were used as the starting point for the ligand-based drug design (see Methods for full molecular modeling details). For the generation of the initial pharmacophore models for each of **6** and **12**, 500 unique conformations were calculated and aligned [25]. This yielded 10 different ligand-based pharmacophore models, and the one with the highest score (0.9311) was used in the large-scale virtual screening investigation. The pharmacophore-derived model is depicted in Fig. 3B, and this consists of two hydrophobic interaction spheres, reflecting both of the lipophilic moieties of the chosen compounds **6** and **12**, two hydrogen bond acceptors (Fig. 3B, red spheres), which describe the interactions with the carbonyl oxygen and with the 5-membered ring nitrogen, and finally one hydrogen bond donor (Fig. 3B, green sphere) relative to the interactions of the amine group attached to the heterocyclic 5-membered ring. The exclusion volume spheres were also created to approximate the steric circumferences of the  $AsI_{fm}$  binding site of these compounds (see Supplementary material Fig. S1 for the full pharmacophore model). The discriminatory performance of the derived pharmacophore model was critically assessed by screening it against both active molecules **6** and **12** and 100 decoy molecules which were generated from both active compounds (50 decoys per active molecule) using the Decoyfinder software [26]. The pharmacophore model successfully identified both active compounds in the correct conformation and none of the available decoy molecules were identified as virtual hits.



**Scheme 2.** Reagents and conditions: (a) NaOH, EtOH or H<sub>2</sub>O or THF, room temperature. (b) NaCNBH<sub>3</sub>, MeOH, room temperature, overnight. (c) TBTU, NMM, DMF, room temperature, overnight.

Subsequently, a large-scale virtual screening campaign was performed by screening a library of approximately 5.5 million commercially available compounds. This library of virtual compounds was prepared as described in the Experimental section. The compounds were aligned with the investigated validated pharmacophore using the alignment method available in the LigandScout program [21,22]. The virtual screening campaign yielded 3200 hit compounds. Several chemical classes were identified as fitting the screening pharmacophore pattern, including: triazines, 9*H*-purines, pyrazolo[3,4-*d*]pyrimidines, 1*H*-benzo[*d*]imidazoles, imidazoles, triazoles, tetrazoles and thiazoles (Scheme 3). The hit compounds were visually inspected for their fit with the pharmacophore model, and the most promising compounds (**15**–**28**) were purchased for further experimental investigations. The results of the inhibition assay performed at 100  $\mu\text{M}$  for selected commercially available compounds (except for compound **16** and **17** measured at 50  $\mu\text{M}$ ) are presented in Table 2 (see also Supplementary material, Table S1 for the origins, details and vendor quality-control procedures for these compounds, and Section 2 for the analysis performed and the purity characterization).

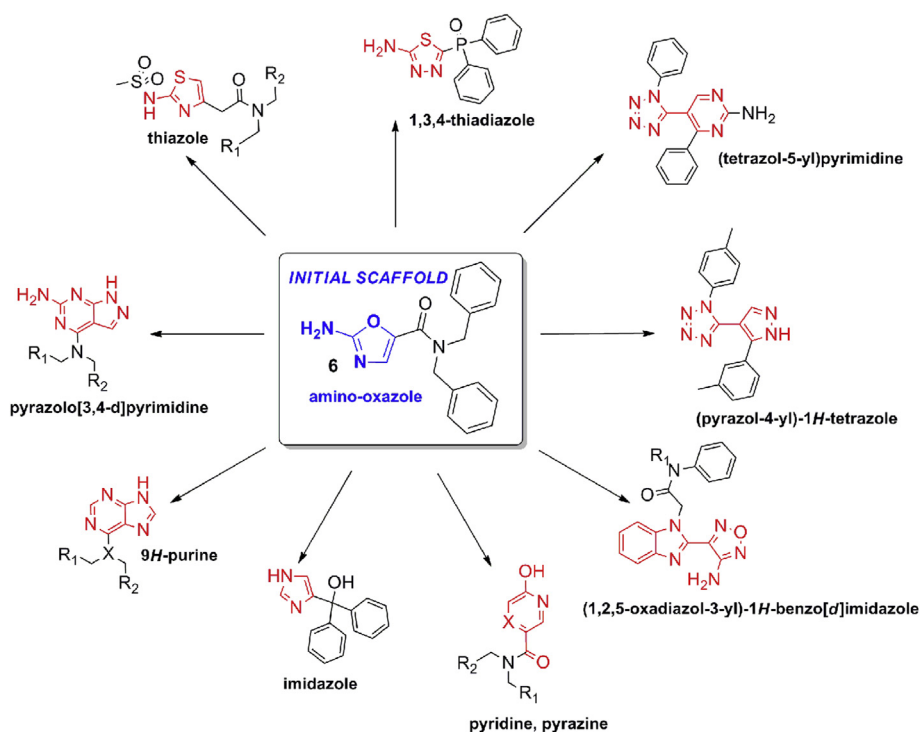
After careful analysis of the conformational alignment to the pharmacophore model of the virtual screening hits obtained, we focused our attention on nine different heterocyclic scaffolds that might serve as replacements for the amino-oxazoles interaction pattern: 7-amino-9*H*-purines (compounds **15**–**18**), 7-amino-1*H*-pyrazolo[3,4-*d*]pyrimidine **19**, 1,3,4-thiadiazol-2-amine **20**, thiazole **21**, imidazole **22**, pyridine-2-ol **23**, pyrazine-2-ol **24**, tetrazoles **25** and **26** and (1,2,5-oxadiazol-3-yl)-1*H*-benzo[*d*]imidazoles **27** and **28** (Scheme 2 and Table 2).

Only compounds from the first two classes were found to be active against the enzyme (Table 2). From the group of 7-amino-9*H*-purines, only compound **18** showed promising inhibitory activity ( $K_i = 3.2 \mu\text{M}$ ), which was comparable to the previously described inhibitor **12** from the series of amino-oxazoles. We can clearly see the importance of only one benzyl group at position 5 of the 7-amino-9*H*-purine scaffold for the inhibitory activity, as none of

the disubstituted compounds (**15**–**17**) showed any inhibition of the target enzyme. 7-Amino-1*H*-pyrazolo[3,4-*d*]pyrimidine **19** was also a moderate inhibitor of  $\text{Asl}_{\text{fm}}$ , with a residual activity of 79% at 100  $\mu\text{M}$ . From the biological activities of the compounds from this series, the importance of the amino group in position 7 can also be established, as it is present in both active compounds **18** and **19**.

The conformation of hit compound **18** that was obtained in the virtual screening procedure is depicted in Fig. 4. The compound contained a 7-amino-9*H*-purine heterocyclic moiety that enabled the fulfillment of the required hydrogen bond acceptor–donor–donor pattern in the pharmacophore model derived for active compounds **6** and **12**. Two alternative positions of the 7-amino-9*H*-purine moiety flipped by 180° in compound **18** were identified by the screening software. Due to the lack of structural information regarding the ATP binding site of  $\text{Asl}_{\text{fm}}$ , it is currently not feasible to differentiate between the derived orientations (Fig. 4). The substituted benzene moiety attached to the 7-amino-9*H*-purine of hit molecule **18** enabled interactions with both hydrophobic spheres. The phenyl moiety was positioned between the hydrophobic spheres, and the chlorine atoms were located in both spheres. It should be noted that since investigated compounds with two lipophilic moieties and containing the same acceptor–donor–donor interaction pattern were inactive in the  $\text{Asl}_{\text{fm}}$  inhibition assays (e.g. compounds **15**–**17**), the potential for another favorable binding placement of an alternative positioning of this hydrophobic moiety within the  $\text{Asl}_{\text{fm}}$  binding site cannot be ruled out. We anticipate that when structural data for the  $\text{Asl}_{\text{fm}}$  enzyme become available, this will be investigated in more detail.

Based on the promising results from the virtual screening campaign, we selected 12 additional commercially available 7-amino-9*H*-purines (compounds **29**–**33**) and 7-amino-1*H*-pyrazolo[3,4-*d*]pyrimidines (compounds **34**–**40**), to provide more information about the SARs of the two discovered compound classes of  $\text{Asl}_{\text{fm}}$  inhibitors. The inhibition of the selected compounds **29**–**40** was assayed at 100  $\mu\text{M}$  and the results are presented in Table 3 (see also Supplementary material, Table S1 for the origins, details and



**Scheme 3.** Different scaffolds identified by the ligand-based virtual screening campaign, as suitable replacements of the amino-oxazole **6** and **12**.

**Table 2**  
Inhibitory activities of the selected commercially available compounds derived from ligand-based virtual screening campaign against Asl<sub>fm</sub>.

Cmpd	Structure	RA [%] <sup>a</sup>	Cmpd	Structure	RA [%] <sup>a</sup>
15		83	22		100
16		94*	23		93
17		110*	24		93
18		47 $K_i = 3.2 \mu\text{M}$	25		92
19		79	26		92
20		95	27		89
21		91	28		116

<sup>a</sup> Residual activity (RA, %) of the enzyme at 100  $\mu\text{M}$  of the tested compound, except for compounds marked with \*, which were tested at 50  $\mu\text{M}$  due to limited solubility. Data are means of two independent experiments. Standard deviations were within  $\pm 10\%$  of the mean.

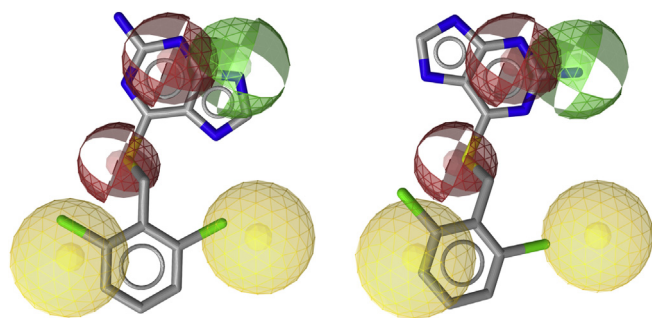


**Fig. 4.** Two of the alternative conformations obtained of the active hit compound **18** from the 7-amino-9H-purine chemical class identified in the virtual screening campaign using the LigandScout ligand-based pharmacophore model (exclusion volumes not shown). The green sphere represents the hydrogen bond donor, and the red spheres hydrogen bond acceptors, while the yellow spheres denote hydrophobic pharmacophoric features. (For interpretation of the references to color in this figure legend, the reader is referred to the web version of this article.)

vendor quality-control procedures for these compounds, and Section 2 for the analysis performed and purity characterization). Among the selected analogs, compounds **30** and **34** were seen to be promising inhibitors of the target enzyme. In the case of the

7-amino-9H-purine scaffold, the importance of a sulfur atom at position 5 is illustrated by the good inhibitory activity of compound **30**. Furthermore, we noted that the 2,6-disubstitution of the phenyl ring is a good choice for inhibitory activity. This could be attributed to the more favorable position of the lipophilic chlorine atoms, and consequently better molecular recognition of the hydrophobic area within the ATP binding site.

Novel active compounds **30** and **34** from the 7-amino-9H-purines and 7-amino-1H-pyrazolo[3,4-d]pyrimidine chemical classes, respectively, were also aligned to the pharmacophore model. These conformations are shown in Supplementary material Fig. S2. Similar observations were made as already described for compound **18**. Again, two flipped positions of the heterocyclic moieties were detected, along with analogous positions of the substituted hydrophobic benzene moiety.

### 2.3. Kinetic determination of inhibitory constants

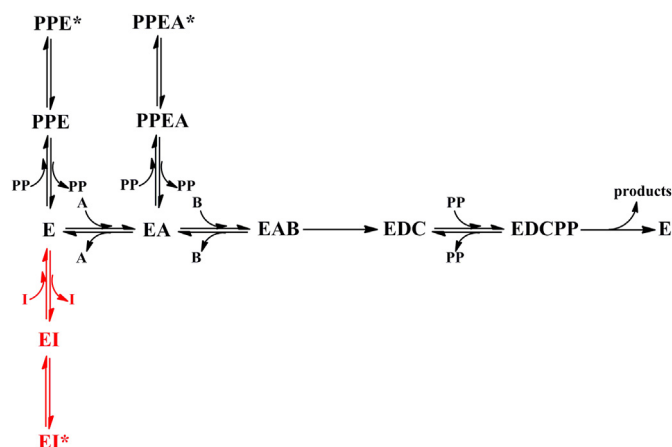
Catalysis by  $Asl_{fm}$  was determined to proceed according to the so-called ter-bi reaction mechanism, as summarized in Scheme 4 [27].

In the first step, the ATP molecule is bound to the enzyme (EA), followed by D-aspartate (EAB). Next, the D-aspartate is

**Table 3**  
Inhibitory activities of commercially available 7-amino-9H-purines (**29–33**) and 7-amino-1H-pyrazolo[3,4-d]pyrimidines (**34–40**) against  $Asl_{fm}$ .

7-amino-9H-purines				7-amino-1H-pyrazolo[3,4-d]pyrimidines			
Cmpd	Y	R <sub>4</sub>	RA [%] <sup>a</sup>	Cmpd	R <sub>5</sub>	R <sub>6</sub>	RA [%] <sup>a</sup>
<b>29</b>	NH		85	<b>34</b>		H	69 <i>K<sub>i</sub></i> = 22 μM
<b>30</b>	S		71 <i>K<sub>i</sub></i> = 35 μM	<b>35</b>		H	86
<b>31</b>	NH		89	<b>36</b>		H	84
<b>32</b>	NH		83	<b>37</b>		H	93
<b>33</b>	NH		84	<b>38</b>		H	88
				<b>39</b>		H	74
				<b>40</b>		CH <sub>3</sub>	87

<sup>a</sup> Residual activity (RA, %) of the enzyme at 100 μM of the tested compound (Cmpd). Data are means of two independent experiments. Standard deviations were within ±10% of the mean.



**Scheme 4.** Putative reaction mechanism of  $Asl_{fm}$ . In the scheme E represents free enzyme, A is ATP, B is D-aspartic acid, C is phosphorylated D-aspartic acid, D is ADP, PP is UDP-MurNAC-pentapeptide and I stands for the inhibitor. The substrates written on the right side represents productive complexes while on the left denotes non-productive complexes. All complexes with asterisk are assumed to evolve upon isomerization.

phosphorylated (EDC) and an amide bond is formed upon the approach of UDP-MurNAC-pentapeptide (EDCPP), by substitution of the phosphate with the  $\epsilon$ -amino group of the lysine at position 3 of UDP-MurNAC-pentapeptide. The catalytic cycle is completed by an ordered release of newly synthesized hexapeptide, ADP and inorganic phosphate. The shape of the curves under continuous measurement suggests that slow conformational changes in  $Asl_{fm}$  go with the binding and release of the participating peptides. Accordingly, the nonproductive binding of UDP-MurNAC-pentapeptide is unmasked when the binding order is violated. In the presence of ATP-competitive inhibitors **6**, **12**, **18**, **30** and **34**, the time course of product formation shows the expected double character: a moderate initial instantaneous decrease in activity is followed by a slow, but substantially stronger, inhibition, which results in sloped asymptotes (see Fig. 5 for selected compounds **6** and **18**).

Kinetic analysis of such a three-substrate reaction, coupled with two additional enzyme reactions for detection, is very complex.

To decrease the number of measurements without sacrificing the amount of information for reliable evaluation, we followed the progress of the reaction in the absence and presence of putative inhibitors for longer periods of time (10–15 min). Subsequently, we analyzed the progress curves obtained with ENZO [28], a web tool written in java, and designed for automatic generation and rapid analysis of data by differential equations from different proposed reaction schemes, with the purpose being to find a suitable one for  $Asl_{fm}$ . In the first step, we analyzed the data in the absence of inhibitors, to obtain characteristic dissociation and rate constants for the  $Asl_{fm}$  reaction itself [40]. In the second step, we fixed the determined constants from the previous step and evaluated only those characteristic for each individual tested inhibitor [41]. The agreement between experimental curves and the theoretical ones as depicted in Fig. 5 for compounds **6** and **18** strongly supports the ATP-competitive effects of investigated compounds (**6**, **12**, **18**, **30**, **34**) all displaying analogous behavior. The estimated inhibition constants are summarized in Tables 1–3.

#### 2.4. Antimicrobial activity

The antimicrobial activities of compounds **6**, **12**, **18**, **30** and **34** were evaluated against three enterococcal strains: *E. faecium* E1679, *E. faecium* E1636 and *E. faecalis* ATTC 29212. For all of these compounds, the minimum inhibitory concentrations (MICs) against all three strains were  $>64 \mu\text{g/mL}$ . The antimicrobial activities of compounds **5–14** were also tested against the clinical strain *E. faecium* D344R in brain-heart infusion agar, using the disk diffusion method. No zone of inhibition was observed. Activity was further assessed in liquid medium using the macrodilution method. No growth inhibition was observed up to the maximal tested concentration (200  $\mu\text{g/mL}$ ), even in the presence of subinhibitory concentrations of ampicillin (2  $\mu\text{g/mL}$ ) (Supplementary material Table S3). The lack of activity of the compounds against these tested bacteria might be due to problems associated with entry into the bacterial cells. As our work presents the initial hit/lead phase of the drug design process the physical properties of these compounds were further assessed by comparing their Clog P and Clog D (at pH = 7.4) values (see Supplementary material Table S4). The range of the observed values between  $-0.5$  and 4 for all compounds

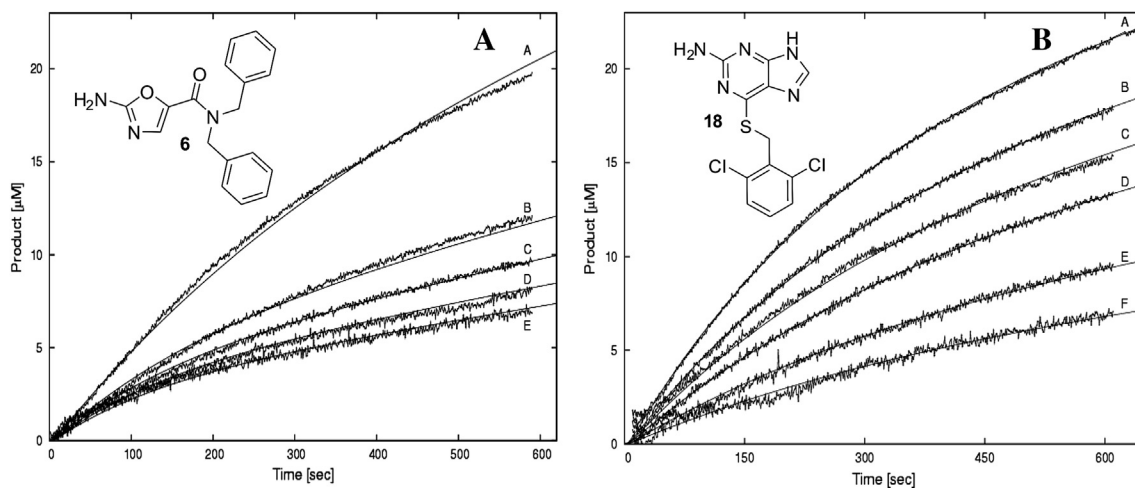


**Fig. 5.** Time courses of product formation in the enzyme reaction by  $Asl_{fm}$  in the absence and presence of inhibitor **6** (A) and **18** (B). The concentrations of **6** (A) were: curve A, zero; B, 50  $\mu\text{M}$ ; C, 75  $\mu\text{M}$ ; D, 100  $\mu\text{M}$ ; and E, 150  $\mu\text{M}$ . The concentrations of **18** (B) were: curve A zero, B 10  $\mu\text{M}$ , C 25  $\mu\text{M}$ , D 50  $\mu\text{M}$ , E 75  $\mu\text{M}$  and 125  $\mu\text{M}$ . The starting concentrations of the reactants were for both cases: 100  $\mu\text{M}$  ATP, 1 mM D-aspartate, 300  $\mu\text{M}$  UDP-MurNAC-pentapeptide, 2 mM phosphoenolpyruvate, 105  $\mu\text{M}$  NADH. The added concentration of  $Asl_{fm}$  was 0.75  $\mu\text{M}$  (**6**) or 1  $\mu\text{M}$  (**18**), and those of pyruvate kinase and lactate dehydrogenase were 0.3 mM and 0.02 mM, respectively. Solid lines indicate the calculated curves based on the ter-bi reaction mechanism using ENZO program [28].

**Table 4**

Determined standard thermodynamic parameters (enthalpy,  $\Delta H_b^0$ , entropy,  $\Delta S_b^0$ , and Gibbs free energy,  $\Delta G_b^0$ ) of the binding of **6** and **18** to AsI<sub>fm</sub>, and the corresponding binding constants,  $K_b$ , obtained by isothermal titration calorimetry.<sup>a</sup>

Cmpd	$\Delta H_b^0/\text{Kcal mol}^{-1}$	$K_b/\text{M}^{-1}$	$K_i/\mu\text{M}$	$\Delta G_b^0/\text{Kcal mol}^{-1}$	$T\Delta S_b^0/\text{Kcal mol}^{-1}$
<b>6</b>	-4.2	$2 \times 10^5$	5	-7.6	3.4
<b>18</b>	-13.8	$2 \times 10^5$	5	-7.6	-6.2

$$^a K_i = 1/K_b, \Delta G_b^0 = RT \ln(K_b/\text{M}^{-1}), \Delta G_b^0 = \Delta H_b^0 - T\Delta S_b^0.$$

except compounds **15** and **17** indicated the drug-like nature of these compounds. Furthermore, as interplay of several additional factors (e.g. permeability, efflux) could be responsible for the lack of activity of these compounds this aspect remains to be investigated in the future.

### 2.5. Biophysical characterization of the hit compounds **6** and **18** by isothermal titration calorimetry

Two of the compounds, **6** and **18**, were tested by isothermal titration calorimetry to obtain thermodynamic parameters of their binding into the AsI<sub>fm</sub> active site at 37 °C. Heat changes upon binding were measured directly, corrected for the heats of dilution, and the model function was fitted to the experimental data points (see Experimental section).

Experiments for the two investigated compounds (**6** and **18**) yielded similar binding constants ( $K_b \approx 10^5 \text{ M}^{-1}$ ) that are in full agreement with their  $K_i$  values (Table 2) obtained in the kinetic analysis using ter-bi reaction mechanism. Interestingly, the ITC results also revealed that the driving forces governing the binding of these two different compound classes differ considerably (Table 4 and Fig. 6). The binding of compound **6** to AsI<sub>fm</sub> results from comparable and favorable enthalpic ( $\Delta H = -4.2 \text{ kcal/mol}$ ) and entropic ( $T\Delta S = 3.4 \text{ kcal/mol}$ ) contributions. On the other hand, the binding of compound **18** is enthalpy driven ( $\Delta H = -13.8 \text{ kcal/mol}$ ) at the temperature investigated, and accompanied by a negative entropy change ( $T\Delta S = -6.2 \text{ kcal/mol}$ ). Nevertheless, compensation of the opposing effects at **18** results in a binding affinity ( $\Delta G_b^0$ ) similar to that of **6**, although there are presumably more non-covalent bonds formed between **18** and the protein than for **6**. Compound **18** obtained in the second drug design stage appears to be more suitable for further optimization, as the increased rigidity of the molecule in its binding conformation should improve the entropy contributions upon retaining the specific and oriented interactions within the AsI<sub>fm</sub> active site [29,30]. Nevertheless, comparing of the Clog P values for compound **6** (Clog P = 2.4) and compound **18** (Clog P = 4.0) a caveat must be stated that subsequent optimization of this compound class must proceed toward

compounds with comparable or preferably lower lipophilicity character. The information that a single dichlorophenyl substituent in compound **18** instead of two phenyl rings in compound **6** yielded comparable inhibitory activity is providing much optimism that affinity of these compounds is not driven purely by lipophilicity. For further rationally-driven optimization of these hits additional structural insights into their molecular recognition by the AsI<sub>fm</sub> enzyme will be of vital importance.

### 3. Conclusions

By combining classical screening and ligand-based pharmacophore modeling approaches in two drug-design stages, we have successfully identified and experimentally characterized the first inhibitors of the bacterial enzyme D-aspartate ligase from *Enterococcus faecium*. Due to the limited knowledge of the structure of AsI<sub>fm</sub>, we focused on the ATP binding site of the enzyme and screened a small collection of known ATP-competitive inhibitors of the large family of the ATP-grasp enzymes. A series of amino-oxazoles and thio-oxazoles derived from bacterial biotin carboxylase inhibitors showed low micromolar activity, with the most potent inhibitor (**12**) with a  $K_i$  of 2.9  $\mu\text{M}$  with respect to ATP. In the second design stage, ligand-based pharmacophore modeling approaches using newly acquired data for the inhibitory activities of the initially discovered series, followed by virtual screening, resulted in identification of new structural types of AsI<sub>fm</sub> inhibitors. This identified novel ATP-competitive inhibitors of AsI<sub>fm</sub> based on 7-amino-9H-purines (**18**) and 7-amino-1H-pyrazolo[3,4-d]pyrimidine (**30** and **34**) scaffolds with  $K_i$  values in the low micromolar range. The binding of two selected inhibitors (**6** and **18**) was subsequently confirmed and studied by isothermal titration calorimetry, with determination of the standard thermodynamic parameters of the inhibitor binding to the enzyme active site. Compounds **6**, **12**, **18**, **30** and **34** have  $K_i$  values in the low micromolar range, and these represent the first inhibitors of AsI<sub>fm</sub> reported to date. We believe that this set of inhibitors discovered here will provide novel lead compounds in antibacterial drug design efforts to combat *E. faecium* infections.

### 4. Experimental section

#### 4.1. Chemistry

Chemicals were obtained from Acros, Aldrich Chemical Co., Apollo Scientific, and Fluka, and they were used without further purification. Analytical thin-layer chromatography was performed on silica gel Merck 60 F<sub>254</sub> precoated plates (0.25 mm), visualized with ultraviolet light, ninhydrin and 2,4-dinitrophenylhydrazine.

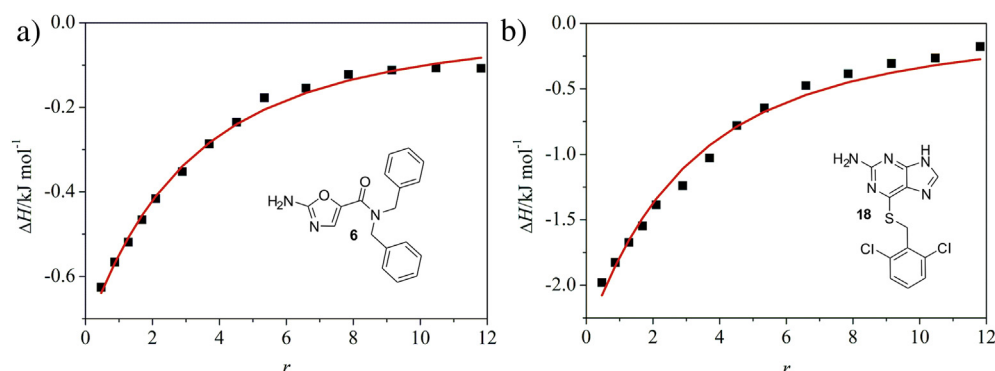


**Fig. 6.** Experimental titration curves and fits according to the single binding site model for binding of compounds **6** (a) and **18** (b) to the AsI<sub>fm</sub> active site at 37 °C. Scheme Caption.

Flash column chromatography was carried out on silica gel 60 (particle size 0.040–0.063 mm; Merck, Germany). Melting points were determined on a Reichert hot-stage microscope and are not corrected.  $^1\text{H}$  NMR spectra were recorded on a Bruker Avance III 400 MHz spectrometer at 295 K and 400 MHz, and are reported in ppm using solvent as internal standard (DMSO- $d_6$  at 2.50 ppm,  $\text{CDCl}_3$  at 7.26 ppm).  $^{13}\text{C}$  NMR spectra were recorded on a Bruker Avance III 400 MHz spectrometer at 295 K and 100 MHz, and are reported in ppm using solvent as the internal standard (DMSO- $d_6$  at 39.5 ppm). Mass spectra data were recorded using a Q-ToF Premier instrument (Waters-Micromass, Manchester, UK). HPLC analyses were performed on an Agilent Technologies HP 1100 instrument, with a G1365B UV–vis detector, a G1316A thermostat, and a G1313A autosampler, using a Phenomenex Luna 5  $\mu\text{M}$  C18 column (4.6 mm  $\times$  150 mm) at a flow rate of 1.0 mL/min. The eluent consisted of 0.1% trifluoroacetic acid in water (A) and methanol (B). The gradient was 20% B to 80% B in 20 min. The purity of the tested compounds was established to be  $\geq 95\%$ .

#### 4.1.1. Synthesis of compound 1

To the suspension of the oxazole ethyl ester (3.13 g, 20.0 mmol) in water, 1 M NaOH (0.04 mL, 40.0 mmol) was added. The mixture was stirred at room temperature for 3 h, and afterward adjusted to pH 2–3 with 1 M HCl. The resulting precipitate **1** was filtered, washed with diethyl ether and dried overnight at 60 °C. Yield: 93%; white crystals, mp 210–212 °C.  $^1\text{H}$  NMR (400 MHz, DMSO- $d_6$ ): 7.01 (s, 2H,  $\text{NH}_2$ ), 7.13 (s, 1H, Ar-H), 12.11 (br s, 1H, COOH) ppm. HRMS (ESI):  $m/z$  [M + H] $^+$  calcd for  $\text{C}_4\text{H}_5\text{N}_2\text{O}_3$  129.1347; found 129.1537.

#### 4.1.2. Synthesis of compound 2

The thiazole ethyl ester (1.0 g, 5.81 mmol) was treated with 0.5 M ethanolic sodium hydroxide solution (60 mL), overnight at room temperature. The reaction mixture was then cooled in an ice bath, and neutralized with acetic acid. The precipitated acid **2** was filtered, washed with diethyl ether, and dried overnight at 60 °C. Yield: 81%; off-white crystals, mp 225–227 °C (lit. [31] 223 °C).  $^1\text{H}$  NMR (400 MHz, DMSO- $d_6$ ): 2.35 (s, 3H,  $\text{CH}_3$ ), 7.61 (s, 2H,  $\text{NH}_2$ ), 12.26 (br s, 1H, COOH) ppm. HRMS (ESI):  $m/z$  [M + H] $^+$  calcd for  $\text{C}_5\text{H}_7\text{N}_2\text{O}_2\text{S}$  159.1698; found 159.1663.

#### 4.1.3. Synthesis of compound 3

To the solution of the thiazole ethyl ester (0.80 g, 4.32 mmol) in THF/water (2:1), NaOH was added (0.65 g, 16.3 mmol), and the reaction mixture was refluxed overnight. THF was removed under reduced pressure and afterward the reaction mixture was neutralized with 1 M HCl. The resulting precipitate **1** was filtered, washed with diethyl ether and dried overnight at 60 °C. Yield: 86%; off-white crystals, mp 168–171 °C (lit. [32] 172–173 °C).  $^1\text{H}$  NMR (400 MHz, DMSO- $d_6$ ):  $\delta$  7.81 (s, 1H, oxazol-H), 8.99 (br s, 2H,  $\text{NH}_2$ ) ppm. HRMS (ESI):  $m/z$  [M + H] $^+$  calcd for  $\text{C}_4\text{H}_5\text{N}_2\text{O}_2\text{S}$  145.1475; found 145.1502.

#### 4.1.4. Synthesis of compound 4

To the solutions of (1H-indol-5-yl)methanamine (0.50 g, 3.42 mmol) and 3,5-dibromobenzaldehyde (0.90 g, 3.42 mmol) in methanol,  $\text{NaCNBH}_3$  (0.43 g, 6.84 mmol) was added, and the mixture was stirred overnight under an argon atmosphere. The solvent was removed under reduced pressure and afterward the residue was dissolved in ethyl acetate (50 mL) and washed with water (3  $\times$  20 mL). The organic phase was dried over  $\text{Na}_2\text{SO}_4$ , and filtered, and the solvent was removed under reduced pressure. The crude product was purified by flash column chromatography using petrolether/ethyl acetate (3:1) as eluent. Yield: 70%, off-white crystals, mp 186–188 °C.  $^1\text{H}$  NMR (400 MHz,  $\text{CDCl}_3$ ):  $\delta$  3.79 (s, 2H,  $\text{CH}_2$ ), 3.91 (s, 2H,  $\text{CH}_2$ ), 6.54–6.59 (m, 1H, indole-H-3), 7.20 (dd,

$J = 8.4, 1.6$  Hz, 1H), 7.25 (t,  $J = 2.7$  Hz, 1H), 7.29 (s, 1H,  $\text{NHCH}_2$ ), 7.40 (d,  $J = 8.4$  Hz, 1H, Ar-H), 7.48 (d,  $J = 2.0$  Hz, 2H, Ar-2,6), 7.57 (t,  $J = 2.0$  Hz, 1H, Ar-4-H), 7.59–7.65 (m, 1H, indole-H), 10.29 (br s, 1H, indole-H-1) ppm. HRMS (ESI):  $m/z$  [M + H] $^+$  calcd for  $\text{C}_{16}\text{H}_{15}\text{N}_2\text{Br}_2$ , 395.1254; found, 395.1259.

#### 4.1.5. Synthesis of compounds 5–14

The suspension of acid (2.00 mmol) in DMF (10 mL) was cooled to 0 °C in an ice bath. *N*-methylmorpholine (0.49 mL, 4.40 mmol) and TBTU (0.84 g, 2.60 mmol) were added, and the reaction mixture was stirred at 0 °C for 0.5 h. Then it was allowed to reach room temperature, and amine (2.00 mmol) was added to the solution. The reaction mixture was stirred overnight at room temperature, after which the solvent was evaporated under reduced pressure. The residue was dissolved in ethyl acetate (40 mL) and washed with a saturated aqueous solution of  $\text{NaHCO}_3$  (3  $\times$  20 mL), 10% citric acid (3  $\times$  20 mL) and brine (20 mL). The organic phase was dried over  $\text{Na}_2\text{SO}_4$ , and filtered, and the solvent was removed under reduced pressure. The crude product was purified by crystallization or flash column chromatography.

**4.1.5.1. 2-Amino-*N*-benzyl-*N*-butyloxazole-5-carboxamide (5).** The crude product was crystallized from  $\text{CH}_2\text{Cl}_2$ . Yield: 46%, off-white crystals, mp 134–137 °C.  $^1\text{H}$  NMR (400 MHz, DMSO- $d_6$ ):  $\delta$  0.85 (t,  $J = 7.4$  Hz, 3H,  $\text{CH}_3$ ), 1.19–1.31 (m, 2H,  $\text{CH}_2\text{CH}_3$ ), 1.45–1.58 (m, 2H,  $\text{CH}_2\text{CH}_2\text{CH}_2$ ), 3.29–3.43 (m, 2H,  $\text{CH}_2\text{CH}_2\text{CH}_2$ ), 4.69 (s, 2H, Ar- $\text{CH}_2$ ), 7.18 (br s, 2H,  $\text{NH}_2$ ), 7.21–7.40 (m, 6H, Ar-H + oxazole-H) ppm.  $^{13}\text{C}$  NMR (400 MHz, DMSO- $d_6$ ):  $\delta$  13.69, 19.45, 29.80, 46.45, 49.28, 127.05, 128.53, 133.81, 137.32, 137.86, 158.04, 162.45 ppm. HRMS (ESI):  $m/z$  [M + H] $^+$  calcd for  $\text{C}_{15}\text{H}_{20}\text{N}_3\text{O}_2$ , 274.1556; found, 274.1547. HPLC  $t_R = 15.965$  min (96.22% at 220 nm, 98.78% at 254 nm).

**4.1.5.2. 2-Amino-*N,N*-dibenzylloxazole-5-carboxamide (6).** The crude product was crystallized from  $\text{CH}_2\text{Cl}_2$ . Yield: 57%, white crystals, mp 216–219 °C.  $^1\text{H}$  NMR (400 MHz, DMSO- $d_6$ ):  $\delta$  5.77 (s, 4H, 2  $\times$   $\text{CH}_2$ ), 7.12 (s, 1H, oxazole-H), 7.18–7.42 (m, 12H, Ar-H +  $\text{NH}_2$ ) ppm.  $^{13}\text{C}$  NMR (400 MHz, DMSO- $d_6$ ):  $\delta$  49.50, 127.03, 127.81, 128.63, 134.40, 136.89, 137.21, 158.47, 162.66 ppm.  $\delta$  HRMS (ESI):  $m/z$  [M + H] $^+$  calcd for  $\text{C}_{18}\text{H}_{18}\text{N}_3\text{O}_2$ , 308.1399; found, 308.1389. HPLC  $t_R = 16.662$  min (98.19% at 220 nm, 99.34% at 254 nm).

**4.1.5.3. 2-Amino-*N,N*-dibutyloxazole-5-carboxamide (7).** The crude product was crystallized from  $\text{CH}_2\text{Cl}_2$ . Yield: 38%, yellow crystals, mp 121–124 °C.  $^1\text{H}$  NMR (400 MHz, DMSO- $d_6$ ):  $\delta$  0.89 (t,  $J = 7.4$  Hz, 6H, 2  $\times$   $\text{CH}_3$ ), 1.22–1.34 (m, 4H, 2  $\times$   $\text{CH}_2\text{CH}_3$ ), 1.45–1.56 (m, 4H,  $\text{CH}_2\text{CH}_2\text{CH}_2$ ), 3.29–3.44 (m, 4H,  $\text{CH}_2\text{CH}_2\text{CH}_2$ ), 7.18 (br s, 2H,  $\text{NH}_2$ ), 7.23 (s, 1H, oxazole-H) ppm.  $^{13}\text{C}$  NMR (400 MHz, DMSO- $d_6$ ): 13.74, 19.52, 30.09, 46.41, 133.14, 137.72, 157.52, 162.22 ppm. HRMS (ESI):  $m/z$  [M + H] $^+$  calcd for  $\text{C}_{12}\text{H}_{22}\text{N}_3\text{O}_2$ , 240.1712; found, 240.1710. HPLC  $t_R = 16.210$  min (98.18% at 220 nm, 98.87% at 254 nm).

**4.1.5.4. 2-Amino-*N,N*-bis(pyridin-2-ylmethyl)oxazole-5-carboxamide (8).** The crude product was purified with flash column chromatography using chloroform/methanol (9:1) as eluent. Yield: 21%, yellow crystals, mp 125–128 °C.  $^1\text{H}$  NMR (400 MHz, DMSO- $d_6$ ):  $\delta$  4.82 (s, 4H, 2  $\times$   $\text{CH}_2$ ), 7.20 (s, 1H, oxazole-H), 7.23–7.40 (m, 6H, pyr-H +  $\text{NH}_2$ ), 7.72–7.82 (m, 2H, pyr-H), 8.49–8.57 (m, 2H, pyr-H) ppm.  $^{13}\text{C}$  NMR (400 MHz, DMSO- $d_6$ ):  $\delta$  2.28, 121.56, 122.41, 134.32, 136.91, 137.01, 149.23, 156.98, 158.60, 162.63 ppm. HRMS (ESI):  $m/z$  [M + H] $^+$  calcd for  $\text{C}_{16}\text{H}_{16}\text{N}_5\text{O}_2$ , 310.1304; found, 310.1309. HPLC  $t_R = 15.965$  min (96.22% at 220 nm, 98.78% at 254 nm).

**4.1.5.5. 2-Amino-*N*-ethyl-*N*-(pyridin-4-ylmethyl)oxazole-5-carboxamide (9).** The crude product was purified with flash column

chromatography using chloroform/methanol (9:1) as eluent. Yield: 39%, pale yellow crystals, mp 162–166 °C.  $^1\text{H}$  NMR (400 MHz, DMSO- $d_6$ ):  $\delta$  1.15 (t,  $J = 6.8$  Hz, 3H,  $\text{CH}_2\text{CH}_3$ ), 3.48 (q,  $J = 6.8$  Hz, 2H,  $\text{CH}_2\text{CH}_3$ ), 4.69 (s, 2H,  $\text{CH}_2$ ), 7.11 (s, 1H, oxazole-H), 7.24 (d,  $J = 6.1$  Hz, pyr-H-3,5), 7.28 (br s, 2H,  $\text{NH}_2$ ), 8.52 (d,  $J = 6.1$  Hz, pyr-H-2,6) ppm.  $^{13}\text{C}$  NMR (400 MHz, DMSO- $d_6$ ):  $\delta$  13.49, 42.35, 48.39, 122.04, 134.17, 137.04, 147.31, 149.68, 157.96, 162.60 ppm. HRMS (ESI):  $m/z$   $[\text{M} + \text{H}]^+$  calcd for  $\text{C}_{12}\text{H}_{15}\text{N}_4\text{O}_2$ , 247.1195; found, 247.1203. HPLC  $t_{\text{R}} = 9.277$  min (97.09% at 220 nm, 98.99% at 254 nm).

**4.1.5.6. 2-Amino-N-(1H-benzo[d]imidazol-2-yl)oxazole-5-carboxamide (10).** The crude product was purified with flash column chromatography using ethyl acetate/methanol (8:1) as eluent. Yield: 26%, off-white crystals, mp > 300 °C.  $^1\text{H}$  NMR (400 MHz, DMSO- $d_6$ ):  $\delta$  7.11 (br s, 2H,  $\text{NH}_2$ ), 7.36–7.51 (m, 5H, Ar-H + oxazole-H), 7.77 (s, 1H, CONH) ppm.  $^{13}\text{C}$  NMR (400 MHz, DMSO- $d_6$ ):  $\delta$  114.6, 123.7, 135.8, 136.2, 142.5, 147.4, 162.7, 166.2 ppm. HRMS (ESI):  $m/z$   $[\text{M} + \text{H}]^+$  calcd for  $\text{C}_{11}\text{H}_{10}\text{N}_5\text{O}_2$ , 244.0834; found, 244.0838. HPLC  $t_{\text{R}} = 18.464$  min (98.65% at 220 nm, 99.09% at 254 nm).

**4.1.5.7. N-((1H-Indol-5-yl)methyl)-2-aminooxazole-5-carboxamide (11).** The crude product was purified with flash column chromatography using chloroform/methanol (9:1) as eluent. Yield: 46%, light-brown crystals, mp 207–211 °C.  $^1\text{H}$  NMR (400 MHz, DMSO- $d_6$ ):  $\delta$  4.44 (d,  $J = 6.0$  Hz, 2H,  $\text{CH}_2$ ), 6.36–6.40 (m, 1H, indole-H-3), 7.08 (dd,  $J = 8.4, 1.6$  Hz, 1H), 7.21 (br s, 2H,  $\text{NH}_2$ ), 7.33–7.42 (m, 2H, oxazole-H + indole-H), 7.45 (s, 1H, indole-H), 7.49 (s, 1H, indole-H), 8.46 (t,  $J = 6.0$  Hz, 1H, CONH), 11.09 (br s, 1H, indole-H-1) ppm.  $^{13}\text{C}$  NMR (400 MHz, DMSO- $d_6$ ):  $\delta$  42.19, 100.85, 111.16, 118.69, 120.97, 125.54, 127.51, 129.81, 131.32, 134.96, 138.36, 156.90, 162.43 ppm. HRMS (ESI):  $m/z$   $[\text{M} + \text{H}]^+$  calcd for  $\text{C}_{13}\text{H}_{13}\text{N}_4\text{O}_2$ , 257.1039; found, 257.1032. HPLC  $t_{\text{R}} = 8.482$  min (98.97% at 220 nm, 99.54% at 254 nm).

**4.1.5.8. N-((1H-Indol-5-yl)methyl)-2-amino-N-(3,5-dibromobenzyl)oxazole-5-carboxamide (12).** The crude product was purified with flash column chromatography using chloroform/ethyl acetate (1:10) as eluent. Yield: 68%, pink crystals, mp 187–191 °C.  $^1\text{H}$  NMR (400 MHz, DMSO- $d_6$ ):  $\delta$  4.62 (s, 2H,  $\text{CH}_2$ ), 4.80 (s, 2H,  $\text{CH}_2$ ), 6.40 (m, 1H, indole-H-3), 6.98 (br s, 2H,  $\text{NH}_2$ ), 7.16 (s, 1H, oxazole-H), 7.27–7.49 (m, 6H, Ar-H), 7.72 (s, 1H, Ar-4'-H), 11.11 (br s, 1H, indole-H-1) ppm.  $^{13}\text{C}$  NMR (400 MHz, DMSO- $d_6$ ):  $\delta$  51.14, 59.75, 101.00, 111.70, 118.64, 120.49, 122.52, 125.83, 126.97, 127.75, 131.96, 134.69, 135.25, 136.83, 140.62, 142.72, 158.47, 162.71 ppm. HRMS (ESI):  $m/z$   $[\text{M} + \text{H}]^+$  calcd for  $\text{C}_{20}\text{H}_{17}\text{N}_4\text{O}_2\text{Br}_2$ , 502.9718; found, 502.9712. HPLC  $t_{\text{R}} = 18.464$  min (98.65% at 220 nm, 99.09% at 254 nm).

**4.1.5.9. 2-Amino-N,N-dibenzylthiazole-5-carboxamide (13).** The crude product was purified with flash column chromatography using ethyl acetate/hexane (1:1) as eluent. Yield: 41%, yellow crystals, mp 114–118 °C.  $^1\text{H}$  NMR (400 MHz, DMSO- $d_6$ ):  $\delta$  4.67 (s, 4H,  $2 \times \text{CH}_2$ ), 7.16 (s, 1H, thiazole-H), 7.21–7.43 (m, 10H, Ar-H), 7.54 (br s, 2H,  $\text{NH}_2$ ) ppm.  $^{13}\text{C}$  NMR (400 MHz, DMSO- $d_6$ ):  $\delta$  50.24, 119.63, 126.99, 127.21, 128.68, 137.14, 142.68, 162.63, 171.61 ppm. HRMS (ESI):  $m/z$   $[\text{M} + \text{H}]^+$  calcd for  $\text{C}_{18}\text{H}_{18}\text{N}_3\text{OS}$ , 324.1171; found, 324.1176. HPLC  $t_{\text{R}} = 18.464$  min (98.65% at 220 nm, 99.09% at 254 nm).

**4.1.5.10. 2-Amino-N,N-dibenzyl-4-methylthiazole-5-carboxamide (14).** The crude product was purified with flash column chromatography using ethyl acetate as eluent. Yield: 53%, yellow crystals, mp 125–128 °C.  $^1\text{H}$  NMR (400 MHz, DMSO- $d_6$ ):  $\delta$  2.21 (s, 3H,  $\text{CH}_3$ ), 4.56 (s, 4H,  $2 \times \text{CH}_2$ ), 7.18–7.48 (m, 13H, Ar-H +  $\text{NH}_2$  + thiazole-H) ppm.  $^{13}\text{C}$  NMR (400 MHz, DMSO- $d_6$ ):  $\delta$  16.67, 49.51, 109.85, 127.31,

128.63, 132.32, 137.06, 151.04, 164.75, 167.77 ppm. HRMS (ESI):  $m/z$   $[\text{M} + \text{H}]^+$  calcd for  $\text{C}_{19}\text{H}_{20}\text{N}_3\text{OS}$ , 338.1327; found, 338.1321. HPLC  $t_{\text{R}} = 15.613$  min (100.0% at 220 nm, 100.0% at 254 nm).

#### 4.2. Ligand-based pharmacophore modeling and virtual screening procedures

Ligand-based pharmacophore modeling and virtual screening were performed using the LigandScout software [21]. The initial constructed conformations of the active compounds **6** and **12** were minimized using the MMFF94 force field, and imported into the ligand-based module available in LigandScout. Five-hundred unique conformations were calculated for each structure by applying the following settings of the LigandScout conformer generator coupled to the OMEGA software: maximum number of output conformers per molecule = 500; RMS threshold to duplicate conformers = 0.4 Å; maximum number of all generated conformers per molecule = 30,000; and maximum number of intermediate conformers per molecule = 4000. Subsequently, the conformers were dynamically aligned [22] to yield 10 ligand-based merged pharmacophore models. A scoring function that combined pharmacophore fit and atom shape overlap was used to assess the models produced. The ligand-based pharmacophore model with the highest score of 0.9311 was selected for further use (see Supplementary material, Fig. S1, for a complete merged Pharmacophore model). Visual inspection revealed that most of the remaining nine derived pharmacophore models closely resembled this model. The initial number of available merged pharmacophoric features was reduced to obtain on the one hand sufficient molecular recognition pattern required for the ligand binding, and to increase on the other hand the chemical space identified by the pharmacophore model [33]. The reduced ligand-based pharmacophore model was used in the large-scale virtual screening campaign. The derived pharmacophore model (see Fig. 3) consisted of two hydrophobic interaction spheres, two hydrogen bond acceptors, and one hydrogen bond donor. Exclusion volume spheres were also added, to approximate the steric circumference of the  $\text{AsI}_{\text{m}}$  binding site. The discriminatory performance of the derived pharmacophore model was validated by a screening experiment against 100 decoy molecules generated for both active compounds **6** and **12** (50 decoys/molecule) using the Decoyfinder software [26]. Decoyfinder generates sets of decoy molecules for defined active ligands. Decoys have similar number of rotational bonds, hydrogen bond acceptors, hydrogen bond donors, log  $P$  value and molecular weight as active molecules but are chemically different, which is defined by a maximum Tanimoto value threshold between active ligand and decoy molecule MACCS fingerprints [26]. The pharmacophore model successfully identified the both active compounds in the correct orientation and none of the generated decoy molecules were identified as potential hits.

The pharmacophore model was used to screen approximately 5.5 million commercially available compounds, all of which were previously converted into multifunctional format (25 conformers for each compound in the database) using the LigandScout screening module. The conformers of the molecules in the screening library were generated using the idbgen module that is available in LigandScout, coupled with the OMEGA software. The default high-throughput settings were used for the library generation: maximum number of output conformers per molecule = 25; RMS threshold to duplicate conformers = 0.8 Å; maximum number of all generated conformers per molecule = 30,000; and maximum number of intermediate conformers per molecule = 4000. In the virtual screening experiments, each compound had to fulfill all of the derived pharmacophore constraints to be identified as a virtual hit. Pharmacophore Fit scoring function was used to score the

matching of the hit molecules to the pharmacophore model [32]. The LigandScout screening procedure retrieved 3200 hit compounds that were carefully visually assessed to identify compound classes, and afterward to select compounds for further inhibition assays.

#### 4.3. Protein expression and purification

DNA of *E. faecium* D359 was amplified with *Pfu* Turbo DNA polymerase (Stratagene, La Jolla, CA) by PCR, using the primers Asl1 (5'-GAGAGACCATGGTGAACAGTATTGAAAATGAAG-3') and Asl2 (5'-CTCCATGGCTAGGATCCTTCTTTCACATGAAAATACTTTG-3'). The PCR product was then digested with *Nco*I and *Bam*HI (underlined) and cloned into pET2818; the resulting plasmid (pSJL1) was introduced into *E. coli* BL21 ( $\lambda$ DE3) harboring the pREP4 plasmid. For protein production, the overnight culture was grown at 37 °C in brain–heart infusion (BHI) broth containing ampicillin (50  $\mu$ g/mL). Five milliliter aliquots of overnight culture were used to inoculate 2 L BHI broth containing ampicillin (50  $\mu$ g/mL) and bacteria grown at 37 °C to an optical density at 600 nm ( $OD_{600}$ ) of 0.7–0.8. Isopropyl- $\beta$ -D-thiogalactopyranoside (IPTG) was added (0.5 mM) and the incubation was continued for 3.5 h at 37 °C. The bacteria were harvested, and lysed by sonication. The Asl<sub>fm</sub> was purified from clarified lysate by affinity chromatography on Ni<sup>2+</sup>-nitriloacetate agarose resin (Sigma–Aldrich) and by filtration (using a HiPrep 16/60 Sephacryl S-200 column, GE Healthcare). Fractions containing the recombinant enzyme were concentrated by ultrafiltration and stored at –20 °C in 50 mM Tris–HCl (pH 8.0), 500 mM NaCl, and 50% glycerol [14].

#### 4.4. Inhibition assay

The target compounds were tested for their inhibition of the D-Asp adding activity of D-aspartate ligase, using the spectrophotometric pyruvate kinase–lactate dehydrogenase enzymatic assay. Each compound was tested in duplicate at 50, 100 and 250  $\mu$ M in a reaction mixture with a final volume of 150  $\mu$ L, containing 100 mM Tris–HCl buffer, pH 8.0, 50 mM MgCl<sub>2</sub>, 2 mM phosphoenolpyruvate, 0.16 mM NADH, 0.3 mM UM5K, 1 mM ATP, 1 mM D-Asp, Triton-114 (0.005%), 2.4 U pyruvate kinase, 3.0 U lactate dehydrogenase, purified His-tagged Asl<sub>fm</sub> and the test compound dissolved in DMSO. The reaction mixture was first incubated at 37 °C for 2 min, and then initiated by the addition of UM5K (0.3 mM). The change in absorbance at 340 nm, which corresponds to ADP formation in the Asl<sub>fm</sub>-catalyzed reaction, was monitored at 37 °C for 10 min using a Perkin Elmer Lambda 45 UV/VIS spectrophotometer. Residual activities were calculated relative to control assays without the compounds and with DMSO.  $K_i$  determinations were performed under similar conditions, using D-Asp (1 mM), ATP (50 and 100  $\mu$ M) and six inhibitor concentrations (depending on the range of its inhibitory activity), with monitoring of the enzymatic reaction for 10 min.

All commercially available compounds with inhibitory activity on Asl<sub>fm</sub> (**18**, **30**, and **34**) were characterized using the HR-MS technique, and their purities were determined by HPLC. The purities of the tested compounds were established as  $\geq 95\%$  (see Supplementary material, Table S2).

#### 4.5. Isothermal titration calorimetry (ITC) measurements

The heat changes upon binding were measured using a VP-ITC microcalorimeter from MicroCal, LLC (Northampton, MA, USA). Purified Asl<sub>fm</sub> stock solution in 10% glycerol was dialyzed for 40 h at 4 °C prior to titration (100 mM Tris–HCl, pH 8.0, 50 mM MgCl<sub>2</sub>, 0.005% Triton X-114). The ligand solutions were prepared by adding

a stock solution of **6** or **18** in DMSO to the dialysis buffer to obtain 50  $\mu$ M solutions of the Asl<sub>fm</sub> inhibitor in 5% DMSO. Successive aliquots of the degassed ligand solutions (11–31  $\mu$ L) were injected at 5–8 min intervals by a motor driven syringe (300  $\mu$ L) into the degassed Asl<sub>fm</sub> solution (approximately 1  $\mu$ M, 5% DMSO) in the calorimeter cell ( $V = 1.386$  mL) with constant stirring (300 rpm) at 37 °C. At the end of experiment, the final ligand:enzyme ratio in the titration cell was about 12:1. The titration data was further corrected for the heat changes observed in the control titration of the ligand solution in the dialysis buffer alone (containing 5% DMSO). The experimental data were analyzed using the Origin 7.0 software, provided by MicroCal, and fitted using a home written program, based on the non-linear Levenberg–Marquardt  $\chi^2$  regression procedure, assuming a single binding site model (two parameters fit) [34]:

$$P + L \rightleftharpoons PL$$

$$\Delta H = \Delta H_b^0 \left( \frac{\partial n_{PL}}{\partial n_2} \right) = \frac{1}{2} \Delta H_b^0 \left( 1 - \frac{r-1 + \left( \frac{1}{K_b [P]_{tot}} \right)}{\sqrt{\left( 1+r + \left( \frac{1}{K_b [P]_{tot}} \right)^2 - 4r \right)}} \right)$$

where  $P$ ,  $L$  and  $PL$  represent Asl<sub>fm</sub>, ligand, and the Asl<sub>fm</sub>–ligand complex, respectively,  $\Delta H$  and  $\Delta H_b^0$  are the measured enthalpy upon aliquot addition and the standard enthalpy change of the binding reaction, respectively,  $n_2$  and  $n_{PL}$  represent the total number of moles of ligand and Asl<sub>fm</sub>–ligand complex in the titration cell,  $r$  is the bound ligand to total protein concentration,  $[P]_{tot}$ , ratio, and  $K_b$  is the binding constant. A detailed explanation of the applied model equation is given in the literature [35].

#### 4.6. Antibacterial activity measurements

The antibacterial activities of the compounds were assessed against *E. faecalis* ATCC 29212 [36], *E. faecium* E1679 [37] and *E. faecium* E1636 [37]. Minimum inhibitory concentrations (MICs) were determined by broth microdilution according to standard methodologies [38].

For the disk diffusion method, the compounds were dissolved in 100% DMSO to a concentration of 20 mg/ml, and 160  $\mu$ g were loaded onto paper disks, which were placed on BHI agar freshly inoculated with *E. faecium* D344R [39]. Bacterial growth was assessed after 18 h of incubation at 37 °C. For the macrodilution method, compounds were diluted to a final concentration of 200  $\mu$ g/mL (400–800  $\mu$ M) in glass tubes containing 2 mL BHI broth. In a second set of tubes, ampicillin (2  $\mu$ g/mL; Euromedex, Souffelweyersheim, France) was added in order to detect putative synergistic effects of the tested compounds with  $\beta$ -lactams. Each tube was inoculated with  $10^7$  CFU/ml of exponentially growing *E. faecium* D344R and incubated for 18 h at 37 °C.

#### Acknowledgments

This work was supported by the Slovenian Research Agency (Grant: P1-0208) and by post-doctoral grant Z1-4111 (A.P.). A. Z. was the recipient of a Bourse de Recherche de la Ville de Paris.

#### Appendix A. Supplementary data

Supplementary data related to this article can be found at <http://dx.doi.org/10.1016/j.ejmech.2013.06.017>.

## References

- [1] H.W. Boucher, G.H. Talbot, J.S. Bradley, J.E. Edwards, D. Gilbert, L.B. Rice, et al., Bad bugs, no drugs: no ESCAPE! an update from the Infectious Diseases Society of America, *Clin. Infect. Dis.* 48 (2009) 1–12.
- [2] R.C. Moellering Jr., Advances in antibacterial therapy, *Transplant. Proc.* 43 (2011) 2441–2442.
- [3] G.J. Patti, S.J. Kim, J. Schaefer, Characterization of the peptidoglycan of vancomycin-susceptible *Enterococcus faecium*, *Biochemistry* 47 (2008) 8378–8385.
- [4] R. Leclercq, E. Derlot, J. Duval, P. Courvalin, Plasmid-mediated resistance to vancomycin and teicoplanin in *Enterococcus faecium*, *N. Engl. J. Med.* 319 (1988) 157–161.
- [5] W. Vollmer, D. Blanot, M.A. de Pedro, Peptidoglycan structure and architecture, *FEMS Microbiol. Rev.* 32 (2008) 149–167.
- [6] D. Mengin-Lecreulx, B. Lemaitre, Structure and metabolism of peptidoglycan and molecular requirements allowing its detection by the *Drosophila* innate immune system, *J. Endotoxin Res.* 11 (2005) 105–111.
- [7] P. Macheboeuf, C. Contreras-Martel, V. Job, O. Dideberg, A. Dessen, Penicillin binding proteins: key players in bacterial cell cycle and drug resistance processes, *FEMS Microbiol. Rev.* 30 (2006) 673–691.
- [8] H. Barretheau, A. Kovac, A. Boniface, M. Sova, S. Gobec, D. Blanot, Cytoplasmic steps of peptidoglycan biosynthesis, *FEMS Microbiol. Rev.* 32 (2008) 168–207.
- [9] K.H. Schleifer, O. Kandler, Peptidoglycan types of bacterial cell walls and their taxonomic implications, *Bacteriol. Rev.* 36 (1972) 407–477.
- [10] T.E. Benson, D.B. Prince, V.T. Mutchler, K.A. Curry, A.M. Ho, R.W. Sarver, et al., X-ray crystal structure of *Staphylococcus aureus* FemA, *Structure* 10 (2002) 1107–1115.
- [11] J.-L. Mainardi, R. Villet, T.D. Bugg, C. Mayer, M. Arthur, Evolution of peptidoglycan biosynthesis under the selective pressure of antibiotics in gram-positive bacteria, *FEMS Microbiol. Rev.* 32 (2008) 386–408.
- [12] W. Staudenbauer, J.L. Strominger, Activation of D-aspartic acid for incorporation into peptidoglycan, *J. Biol. Chem.* 247 (1972) 5095–5102.
- [13] W. Staudenbauer, E. Willoughby, J.L. Strominger, Further studies of the D-aspartic acid-activating enzyme of *Streptococcus faecalis* and its attachment to the membrane, *J. Biol. Chem.* 247 (1972) 5289–5296.
- [14] S. Bellais, M. Arthur, L. Dubost, J.-E. Hugonnet, L. Gutmann, J. van Heijenoort, et al., Asl<sub>fm</sub>, the D-aspartate ligase responsible for the addition of D-aspartic acid onto the peptidoglycan precursor of *Enterococcus faecium*, *J. Biol. Chem.* 281 (2006) 11586–11594.
- [15] M.Y. Galperin, E.V. Koonin, A diverse superfamily of enzymes with ATP-dependent carboxylate-amine/thiol ligase activity, *Protein Sci.* 6 (1997) 2639–2643.
- [16] S. Dutka-Malen, C. Molinas, M. Arthur, P. Courvalin, Sequence of the vanC gene of *Enterococcus gallinarum* BM4174 encoding a D-alanine:D-alanine ligase-related protein necessary for vancomycin resistance, *Gene* 112 (1992) 53–58.
- [17] V. Škedelj, T. Tomašić, L.P. Mašič, A. Zega, ATP-binding site of bacterial enzymes as a target for antibacterial drug design, *J. Med. Chem.* 54 (2011) 915–929.
- [18] I. Mochalkin, J.R. Miller, L. Narasimhan, V. Thanabal, P. Erdman, P.B. Cox, et al., Discovery of antibacterial biotin carboxylase inhibitors by virtual screening and fragment-based approaches, *ACS Chem. Biol.* 4 (2009) 473–483.
- [19] J.E. Lindsley, Use of a real-time, coupled assay to measure the ATPase activity of DNA topoisomerase II, *Methods Mol. Biol.* 95 (2001) 57–64.
- [20] W.R. McClure, A kinetic analysis of coupled enzyme assays, *Biochemistry* 8 (1969) 2782–2786.
- [21] B. Hess, B. Wurster, Transient time of the pyruvate kinase–lactate dehydrogenase system of rabbit muscle in vitro, *FEBS Lett.* 9 (1970) 73–77.
- [22] T. Langer, R.D. Hoffmann, *Pharmacophores and Pharmacophore Searches*, Wiley VCH, Weinheim, Germany, 2006.
- [23] A. Perdihi, A. Kovac, G. Wolber, D. Blanot, S. Gobec, T. Solmajer, Discovery of novel benzene 1,3-dicarboxylic acid inhibitors of bacterial MurD and MurE ligases by structure-based virtual screening approach, *Bioorg. Med. Chem. Lett.* 19 (2009) 2668–2673.
- [24] G. Wolber, T. Langer, LigandScout: 3-D pharmacophores derived from protein-bound ligands and their use as virtual screening filters, *J. Chem. Inf. Model* 45 (2005) 160–169.
- [25] G. Wolber, A.A. Dornhofer, T. Langer, Efficient overlay of small organic molecules using 3D pharmacophores, *J. Comput. Aided Mol. Des.* 20 (2006) 773–788.
- [26] A. Cereto-Massague, L. Guasch, C. Valls, M. Mulero, G. Pujadas, S. Garcia-Valle, DecoyFinder: an easy-to-use python GUI application for building target-specific decoy sets, *Bioinformatics* 28 (2012) 1661–1662.
- [27] V. Škedelj, et al., in press.
- [28] S. Bevc, J. Konc, J. Stojan, M. Hodošček, M. Penca, M. Praprotnik, et al., ENZO: a web tool for derivation and evaluation of kinetic models of enzyme catalyzed reactions, *PLoS One* 6 (2011) e22265.
- [29] E. Edink, C. Jansen, R. Leurs, R. de Esch, The heat is on: thermodynamic analysis in fragment-based drug discovery, *Drug Discov. Today Technol.* 7 (2010) 189–201.
- [30] J.E. Ladbury, G. Klebe, E. Freire, Adding calorimetric data to decision making in lead discovery: a hot tip, *Nat. Rev. Drug Discov.* 9 (2010) 23–27.
- [31] W. Knauf, Chemotherapeutic nitro heterocycles. XXII. Synthesis and antimicrobial activity of 2-nitrothiazole-5-carboxamide, *Eur. J. Med. Chem.* (1975) 533–534.
- [32] K.E. Rao, Y. Bathini, J.W. Lown, Synthesis of novel thiazole-containing DNA minor groove binding oligopeptides related to the antibiotic distamycin, *J. Org. Chem.* 55 (1990) 728–737.
- [33] J. Kirchmair, P. Markt, S. Distinto, G. Wolber, T. Langer, Evaluation of the performance of 3D virtual screening protocols: RMSD comparisons, enrichment assessments, and decoy selection—what can we learn from earlier mistakes? *J. Comput. Aided Mol. Des.* 22 (2008) 213–228.
- [34] W.H. Press, B.P. Flannery, S.A. Teukolsky, W.T. Vetterling, *Numerical Recipes*, Cambridge University Press, Oxford, 1992.
- [35] V. Škedelj, Emilija Arsovska, T. Tomašić, Ana Kroflič, Vesna Hodnik, Martina Hrast, et al., 6-Arylpyrido[2,3-d]pyrimidines as novel ATP-competitive inhibitors of bacterial D-Alanine:D-Alanine ligase, *PLoS One* (2012) e39922.
- [36] M.-T. Arias-Moliz, P. Baca, S. Ordóñez-Becerra, M.-P. González-Rodríguez, C.-M. Ferrer-Luque, Eradication of enterococci biofilms by lactic acid alone and combined with chlorhexidine and cetrimide, *Med. Oral Patol. Oral Cir. Bucal* (2012).
- [37] W. van Schaik, J. Top, D.R. Riley, J. Boekhorst, J.E.P. Vrijenhoek, C.M.E. Schapendonk, et al., Pyrosequencing-based comparative genome analysis of the nosocomial pathogen *Enterococcus faecium* and identification of a large transferable pathogenicity island, *BMC Genomics* 11 (2010) 239.
- [38] National Committee for Clinical Laboratory Standards (NCCLS), *Methods for Dilution Antimicrobial Susceptibility Tests for Bacteria that Grow Aerobically*, fourth ed., vol. 17, 1997.
- [39] W. Zorzi, X.Y. Zhou, O. Dardenne, J. Lamotte, D. Raze, J. Pierre, et al., Structure of the low-affinity penicillin-binding protein 5 PBP5<sub>fm</sub> in wild-type and highly penicillin-resistant strains of *Enterococcus faecium*, *J. Bacteriol.* 178 (1996) 4948–4957.
- [40] A typical run in the absence of inhibitors was implemented under the following project number enzo.cmm.ki.si/kinetic.php?uwd=120727444&load=true (click 'Set Parameters' and 'Start').
- [41] See enzo.cmm.ki.si/kinetic.php?uwd=120326994&load=true for compound 6; click 'Set Parameters' and 'Start'.